Breakdown of Dynamic Scaling in Thin Film Binary Liquids Undergoing Phase Separation

Hyun-joong Chung and Russell J. Composto*

Materials Science and Engineering and Laboratory for Research on the Structure of Matter, University of Pennsylvania, Philadelphia, Pennsylvania 19104-6272, USA

(Received 24 October 2003; published 6 May 2004)

The kinetics of phase separation in thin polymer blend films displaying discrete and bicontinuous domain morphologies are examined. For discrete domains, the correlation length ξ grows as $t^{1/3}$, in agreement with a coalescence model. By plotting ξ/d vs t/t_i (initiation time), universal growth behavior is obtained for thickness values (d) from 1000 to 190 nm. In contrast, bicontinuous domains grow with a decreasing exponent, 0.62 to 0.28, as d decreases from 900 to 90 nm (i.e., no universal growth). This slowing down with reduced dimensionality suggests suppression of lateral hydrodynamic pumping.

DOI: 10.1103/PhysRevLett.92.185704 PACS numbers: 64.70.Ja, 68.05.–n, 68.15.+e, 68.55.–a

Spinodal decomposition describes the spontaneous separation of a binary fluid mixture into two coexisting phases. A dynamic scaling hypothesis proposes that a dominant length scale characterizes domain growth at the late stage, $R(t) \sim t^{\alpha}$ [1]. Using $R(t) = 2\pi \int S(k,t)dk / \int kS(k,t)dk$, where $S(k,t)$ is the density autocorrelator [2], the length scale can be defined as $\xi(t) = 2\pi/k_{\max}(t)$, where $k_{\max}(t)$ is the dominant peak wave vector of $S(k,t)$. Scaling arguments have been used to predict the growth exponent α during late stage coarsening [3–7]. Whereas discrete droplet domains scale as $\alpha = 1/3$ in 3D [3–6], percolation of the minority phase is proven to accelerate phase separation in fluids resulting in $\alpha = 1$ in the viscous hydrodynamic regime [3,8]. Because of its fundamental and technological relevance, phase separation in 2D binary fluids has been investigated both theoretically and experimentally [2,9–14]. In practice, however, phase separation in real thin film systems is greatly complicated by preferential wetting [15], minority phase percolation, and confinement. Here, we show how the interplay between wetting, percolation, and confinement influences phase separation kinetics in a pseudo-2D system. Thus, our experiments provide a guideline for identifying the key phenomena to be included in next generation theories of phase separation kinetics in 2D binary liquids.

We recently identified the three stages of morphology evolution displayed by 50:50 (bulk) films (495 nm) of deuterated poly(methyl methacrylate) (dPMMA): poly(styrene-*ran*-acrylonitrile) (SAN) at a deep quench [15]. During the early stage (ES), spinodal decomposition produces a bicontinuous morphology, which provides a pathway for the hydrodynamic-flow-driven wetting of dPMMA to the free surface and substrate [16]. When the capillary diameters approach the thickness of the SAN-rich middle layer, phase separation undergoes a transition from 3D to pseudo-2D growth, defining the onset of the intermediate stage (IS). During the IS, dPMMA-rich tubes bridging the two wetting layers continue to coarsen until the middle layer ruptures due to fluctuations at the wetting layer/midlayer interface [17]. During the late stage (LS), a rough film forms with SAN-rich droplets encapsulated by dPMMA-rich wetting layers. The present study focuses on the pattern evolution within the midlayer during the IS.

In this Letter, domain growth of discrete and bicontinuous morphologies is monitored as a function of time in thin films undergoing phase separation. For bulk systems, previous studies have shown that minority phase percolation can activate a hydrodynamic pumping mechanism resulting in fast growth dynamics, $\alpha = 1$ [3,8]. By imaging the internal morphology using atomic force microscopy (AFM), we demonstrate that percolation also accelerates domain growth in pseudo-2D films. In particular, the effect of film thickness (d) on the growth dynamics of discrete and bicontinuous morphologies is investigated over a range of d. Discrete domains display a growth exponent of $1/3$, whereas bicontinuous domains fail to obey any scaling rule. In the latter case, α decreases from 0.62 to 0.28 as d decreases. By normalizing ξ and t by d, universal growth is observed for discrete domains but not for bicontinuous domains.

Polymer mixtures of PMMA and SAN with 33 wt % of AN have been investigated. The weight average molecular weights and polydispersities of PMMA and SAN are 82.5 K and 1.05, and 118 K and 2.24, respectively. This blend displays lower critical solution behavior with a critical temperature of $\sim$160 °C. At 185 °C, the coexisting compositions are nearly pure PMMA and SAN [18]. Thus, instead of PMMA rich and SAN rich, we simplify the nomenclature to PMMA and SAN, respectively. The polymers were dissolved in methyl isobutyl ketone, spun cast on silicon $\langle 100 \rangle$ and then dried at 120 °C in vacuum for 24 h. Films were smooth (rms roughness $<$0.3 nm) and completely homogeneous. The ellipsometric film thickness (d) ranged from 90 to 1000 nm. Samples were annealed on a hot-stage (Mettler FP-82, Mettler Toledo) at 185 °C in argon. The surface and interface morphologies were investigated using a Dimension 3000 AFM (Digital Instruments, Inc.) driven in tapping mode. To

reveal the morphology of the midlayer, PMMA was selectively removed by exposing samples to UV-ozone (6 to 20 min) and/or 2 MeV He^+ (2 to 5 μC) followed by immersion in acetic acid. To ensure consistency, scans of the internal morphology (up to 100^2 μm^2) were taken from several regions and then converted into reciprocal space using a 2D fast Fourier transform (FFT). Radial averaging of the FFT spectrum yielded a peak at k_{max}, which was used to determine the in-plane correlation length between domains, ξ.

Figure 1 shows representative AFM images of the interface morphology for PMMA:SAN films with different bulk compositions 50:50 (left) and 70:30 (right), but similar d, 700 and 630 nm, respectively. The white (high) and dark (black) regions correspond to SAN domains and the Si substrate (i.e., etched PMMA phase), respectively. Clearly, the PMMA phase forms discrete dropletlike domains in the 50:50 blends, and continuous, irregular-shaped domains in the 70:30 system. The terms "discrete growth" (i.e., PMMA domains are disklike) and "bicontinuous growth" will be used to describe phase evolution of the 50:50 and 70:30 blends, respectively. These results are somewhat unexpected because the bulk compositions predict the 50:50 and 70:30 blends to have bicontinuous and discrete structures, respectively. This conundrum can be explained by accounting for the preferential wetting of PMMA, which depletes the midlayer of PMMA and pushes the midlayer compositions into the off-critical and critical regimes, respectively. To test this hypothesis, the area fraction (A_d) of PMMA was determined from the images in Fig. 1. For 50:50 and 70:30 blends, A_d ranged from 20% to 30% and 45% to 55%, respectively. Thus, the discrete and bicontinuous growth are consistent with the off-critical and critical compositions of the midlayer, respectively.

A comparison of the images in Fig. 1 shows that the discrete morphology evolves more slowly than the bicontinuous one, suggesting different growth mechanisms. Figures 2(a) and 2(b) show how the correlation length, ξ, increases with time during the IS for the 50:50 and 70:30 blends, respectively. For both 50:50 and 70:30 blends at a given time, ξ decreases as d decreases, suggesting that confinement reduces domain size. Scaling exponents of 1/3 and 2/3 are plotted as dashed lines in Figs. 2(a) and 2(b). For discrete growth, α values are $\sim 1/3$ for all d, whereas for bicontinuous growth α

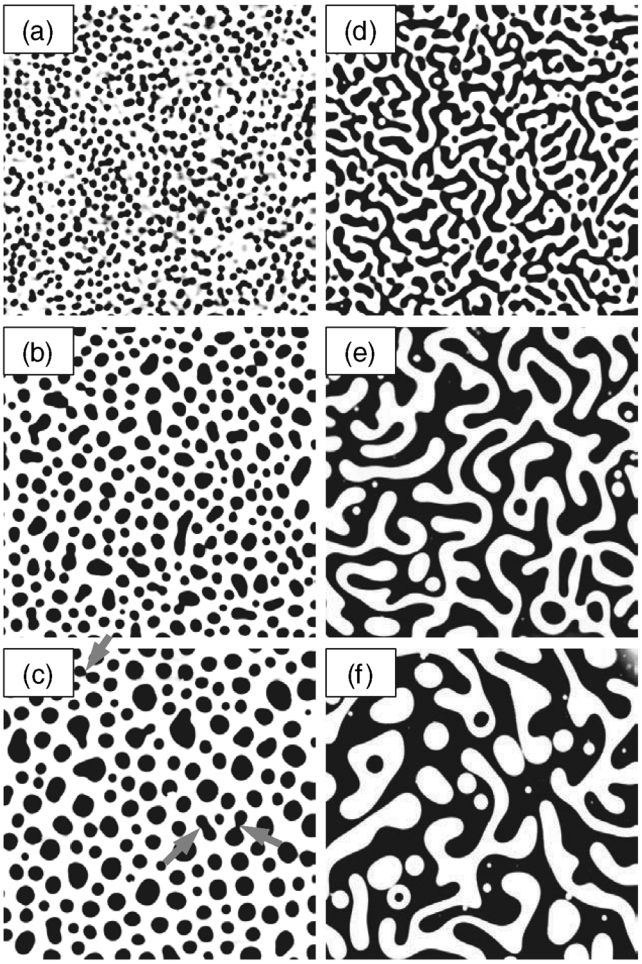

FIG. 1. AFM images of the SAN-rich phase (white) for discrete (700 nm, left column) and bicontinuous (630 nm, right column) growth mechanisms after selective etching of PMMA (dark). The annealing times are [(a), (d)] 360 min, [(b), (e)] 1440 min, and [(c), (f)] 4320 min. Arrows indicate coalescing domains. Image areas are 40^2 μm^2.

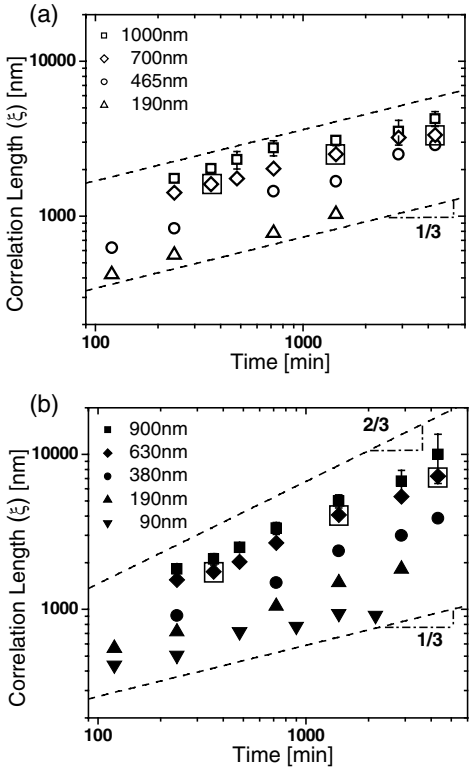

FIG. 2. In-plane domain correlation length, ξ, as a function of time and film thickness for (a) discrete and (b) bicontinuous morphology. Broken lines are to guide the eye. Symbols within open squares correspond to images in Fig. 1.

decreases from 0.62 to 0.28 as d decreases 900 to 90 nm. To confirm that the discrete growth exponent is $\alpha = 1/3$, ξ^3 was plotted (not shown) and found to increase linearly with t. In contrast, ξ^3 deviated from linearity for bicontinuous growth, particularly at large d. Thus, confinement affects the phase evolution of the bicontinuous morphology differently than the discrete morphology, and breaks dynamic scaling.

In previous studies on 50:50 (bulk) thin film polymer blends, surface roughening [17] and film rupture [19] have been related to the degree of confinement, d. Here, we examine if universal scaling is obtained by normalizing ξ and t by d. Because ξ becomes comparable to d at the onset of the IS (i.e., crossover from 3D to 2D) [17], ξ has been normalized by d. To normalize t, the onset time for the IS, t_i, is chosen, and t_i is proportional to d as noted next. During the ES, PMMA flows through capillaries to the surface/substrate by hydrodynamic pumping, resulting in a wetting layer growth, $l \propto t^1$ [16]. Concurrently, the midlayer thickness, h, thins. As capillaries coarsen, they eventually form domains that bridge the surface and substrate wetting layers. Once the domain diameter becomes bigger than h, the Laplace pressure (P_σ) within the tube becomes less than P_σ in the wetting layers. The PMMA backflow into the domains (cf. Fig. 9 of Ref. [15]) defines the onset of the IS, t_i, and results in a slowing down of surface roughening [17]. In this study, t_i is measured experimentally from the roughness and described by $t_i[\text{min}] = \frac{1}{2}d[\text{nm}]$. Because $l \propto t^1$ and $h \sim d$ at t_i, then $t_i \propto d$. Thus, if domain growth is universal during the IS, the ξ vs t data shown in Fig. 2 should reduce to a master curve when plotted as ξ/d vs t/t_i.

Figures 3(a) and 3(b) show the scaled domain growth for the discrete and bicontinuous morphologies, respectively. For the discrete growth, the data collapse onto a master curve with a reduced time exponent of 1/3. The dashed line in Fig. 3(a) represents $(\xi/d) = K(t/t_i)^{1/3}$, where K is the proportionality constant. Using $t_i \propto d$, one obtains $\xi \propto d^{2/3}t^{1/3}$. One interpretation of the $t^{1/3}$ scaling is that smaller PMMA domains shrink and the larger ones grow via material transport through the thin wetting layers [3,10]. Alternatively, domain coalescence also predicts $t^{1/3}$ scaling. Modifying the approach by Tanaka [20], domain coalescence can be described as the following. In this mechanism, the SAN domains are viewed as tubes that are squeezed by the disklike PMMA domains. The maximum curvature of the tube occurs when the interdomain distance is a minimum (a_{min}). The resulting pressure gradient produces a Poiseuille flow, causing the PMMA domains to attract each other. This flow is described by the Navier-Stokes equation

$$\eta[\partial^2 v/\partial y^2 + \partial^2 v/\partial z^2] = dP/dx, \qquad (1)$$

where v is the flow velocity along the tube axis or x, η is the viscosity, and P is the pressure. The coordinates y and z are perpendicular to the tube and substrate, respectively.

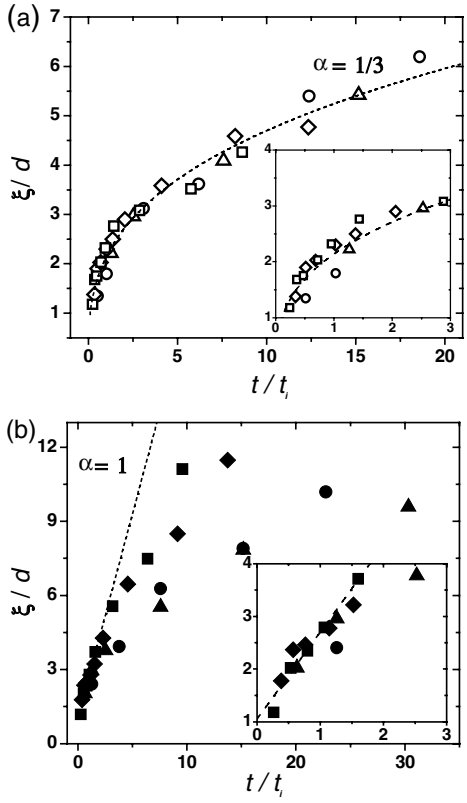

FIG. 3. Reduced correlation length, ξ/d, as a function of reduced time, t/t_i, for (a) discrete and (b) bicontinuous morphologies, where t_i is the onset of the intermediate stage. Insets expand early time behavior. The legend follows Fig. 2.

Scaling analysis gives $\partial^2/\partial z^2 \sim h^{-2} \sim d^{-2}$ and $\partial^2/\partial y^2 \sim a_{\text{min}}^{-2} \sim \xi^{-2}$. From mass conservation, v generates a domain velocity v_d that scales with $d\xi/dt$ [7]. Because $\xi/d > 1$ during the IS [cf. Fig. 3(a)], the left-hand side of (1) reduces to $\eta\xi/(d^2 t)$. The characteristic flow length (L) can be estimated from the in-plane domain radius so $L \sim \xi$ [20]. Using $\Delta P \sim \sigma/r$, where σ is the interfacial tension and r is the radius of curvature ($\sim a_{\text{min}}$), the right-hand side of (1) scales with σ/ξ^2. Therefore, Eq. (1) predicts $\xi \sim (\sigma/\eta)^{1/3} d^{2/3} t^{1/3}$, which accurately captures the scaling exponents for d and t found in Fig. 3(a). Direct evidence for domain coalescence is shown by the arrows in Fig. 1(c).

In contrast to the discrete morphology, the bicontinuous structure obeys universal behavior only for $\xi/d < 3$ as shown in Fig. 3(b). Using mass conservation and an elliptic cross section, the tube width is about twice its height when $\xi/d = 3$. The ratio ξ/d represents the extent of tube anisotropy. As tube anisotropy increases ($\xi/d > 3$), the rate of coarsening slows down as d decreases and dynamic scaling breaks down as shown in Fig. 3(b). One explanation for this breakdown is that hydrodynamic pumping through the SAN tubes is suppressed by confinement. Direct evidence for "in-plane" SAN tubes as well as "necked" tubes is given by the AFM image in Fig. 4. Coarsening occurs by hydrodynamic pumping of SAN

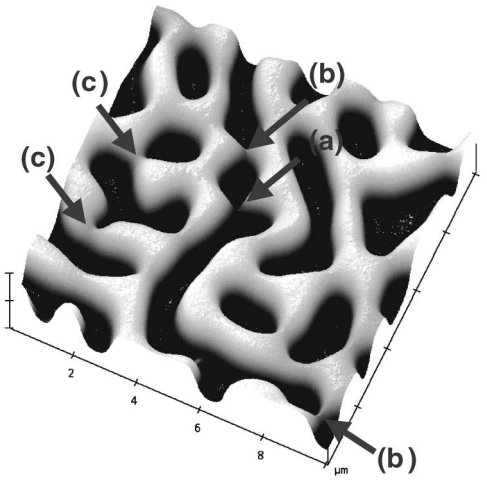

FIG. 4. An AFM prospective plot of the in-plane tube morphology of the SAN-rich phase (light). The film thickness and annealing time are 630 nm and 8 h. PMMA has been removed (dark). The arrows denote (a) a ruptured tube, (b) tubes about to break, and (c) tubes with necked regions. The vertical ticks are 300 nm.

away from necks (arrows *b* and *c*) leading to tube rupture (arrow *a*). Because the tubes are pseudo-2D, a strict 2D linear stability analysis is not possible [10]. We propose a possible reason for the breakdown of dynamic scaling. If the necked regions are opposed by a viscoelastic stress [21] that increases as the tube approaches the surface/substrate (i.e., thinner l), coarsening will tend to slow down as d decreases. The origin of this stress may be related to the suppression of tube fluctuations near the interfaces, particularly for thin wetting layers (small d) which require a high penalty to deform the air/polymer surface. The discrete growth is not retarded by this mechanism because its kinetics is controlled by domain attraction or diffusion, which are slow mechanisms (i.e., $\alpha = 1/3$).

Several studies support the idea that confinement can suppress the hydrodynamic pumping mechanism. One study [22] reported that the viscoelastic dynamics of short (unentangled) chains display a rubberlike elasticity when confined below $4R_g$. Similarly, diffusion of confined entangled polymers was an order of magnitude slower than bulk values even for films $\sim 10R_g$ from the substrate [23]. Numerical studies of phase separating viscoelastic liquids show that enhanced elasticity suppresses hydrodynamic interactions, leading to a smaller α [21]. An increase in viscosity due to confinement cannot explain why α decreases because α is determined only by the growth mechanism. Thus, studies are needed to elucidate the connection between viscoelastic behavior under confinement and phase separation in thin films.

In summary, AFM is used to show that polymer blend films undergoing phase separation and wetting can display discrete (50:50) or bicontinuous (70:30) growth mechanisms. For discrete growth, universal behavior is obtained by plotting ξ/d (thickness) vs t/t_i (initiation time) for d from 1000 to 190 nm. A coalescence-based model captures the experimental scaling relations, $\xi \propto d^{2/3}t^{1/3}$. For bicontinuous growth, universal behavior is not observed, $\xi \propto t^{\alpha}$, where α decreases from 0.62 to 0.28 as d decreases from 900 to 90 nm, respectively. The slowing down of phase growth suggests that lateral hydrodynamic pumping that drives phase coarsening is suppressed by film confinement. We hope that these new experimental results will motivate the development of new theories that describe the breakdown of dynamic scaling in thin film binary liquids undergoing bicontinuous growth.

We thank Professors H. Wang (MTU) and B.-M. Zhang Newby (Akron) for insightful discussions. This work was supported by the National Science Foundation.

*Author to whom correspondence should be addressed. Electronic address: composto@lrsm.upenn.edu

[1] J. D. Gunton, M. San Miguel, and P. S. Sahni, in *Phase Transitions and Critical Phenomena*, edited by C. Domb and J. L. Lebowitz (Academic, New York, 1983), Vol. 8.
[2] A. J. Wagner and M. E. Cates, Europhys. Lett. **56**, 556 (2001).
[3] E. D. Siggia, Phys. Rev. A **20**, 595 (1979).
[4] I. M. Lifshitz and V. V. Slyozov, J. Phys. Chem. Solids **19**, 35 (1961).
[5] K. Binder and D. Stauffer, Phys. Rev. Lett. **33**, 1006 (1974).
[6] H. Tanaka, J. Chem. Phys. **105**, 10 099 (1996).
[7] H. Furukawa, Phys. Rev. A **31**, 1103 (1985).
[8] N.-C. Wong and C. M. Knobler, Phys. Rev. A **24**, 3205 (1981).
[9] J. Chin and P. V. Coveney, Phys. Rev. E **66**, 016303 (2002).
[10] M. San Miguel, M. Grant, and J. D. Gunton, Phys. Rev. A **31**, 1001 (1985).
[11] W. R. Osborn *et al.*, Phys. Rev. Lett. **75**, 4031 (1995).
[12] Y. Wu *et al.*, Phys. Rev. Lett. **74**, 3852 (1995).
[13] C. K. Haas and J. M. Torkelson, Phys. Rev. Lett. **75**, 3134 (1995).
[14] L. Sung *et al.*, Phys. Rev. Lett. **76**, 4368 (1996).
[15] H. Wang and R. J. Composto, J. Chem. Phys. **113**, 10 386 (2000).
[16] H. Wang and R. J. Composto, Phys. Rev. E **61**, 1659 (2000).
[17] H. Wang and R. J. Composto, Macromolecules **35**, 2799 (2002).
[18] B. Z. Newby and R. J. Composto, Macromolecules **33**, 3274 (2000).
[19] H. Hoppe, M. Heuberger, and J. Klein, Phys. Rev. Lett. **86**, 4863 (2001).
[20] H. Tanaka, J. Phys. Condens. Matter **13**, 4637 (2001).
[21] T. Taniguchi and A. Onuki, Phys. Rev. Lett. **77**, 4910 (1996).
[22] H.-W. Hu and S. Granick, Science **258**, 1339 (1992).
[23] X. Zheng *et al.*, Phys. Rev. Lett. **79**, 241 (1997).